# Deposition of environmentally relevant nanoplastic models in sand during transport experiments

Alice Pradel, Hind El Hadri, Cloé Desmet, Jessica Ponti, Stephanie Reynaud, Bruno Grassl, Julien Gigault

# Journal Pre-proof

Deposition of environmentally relevant nanoplastic models in sand during transport experiments

Alice Pradel, Hind el Hadri, Cloé Desmet, Jessica Ponti, Stéphanie Reynaud, Bruno Grassl, Julien Gigault

Please cite this article as: Pradel, A., Hadri, H.e., Desmet, Cloé., Ponti, J., Reynaud, Sté., Grassl, B., Gigault, J., Deposition of environmentally relevant nanoplastic models in sand during transport experiments, *Chemosphere* (2020), doi: https://doi.org/10.1016/j.chemosphere.2020.126912.

This is a PDF file of an article that has undergone enhancements after acceptance, such as the addition of a cover page and metadata, and formatting for readability, but it is not yet the definitive version of record. This version will undergo additional copyediting, typesetting and review before it is published in its final form, but we are providing this version to give early visibility of the article. Please note that, during the production process, errors may be discovered which could affect the content, and all legal disclaimers that apply to the journal pertain.

**Deposition of Environmentally Relevant Nanoplastic Models in Sand during Transport**

**Experiments**

Alice Pradel [a*], Hind el Hadri [b], Cloé Desmet[c], Jessica Ponti[c], Stéphanie Reynaud [b], Bruno Grassl [b], Julien Gigault [a*]

[a] *Univ Rennes, CNRS, Géosciences Rennes - UMR 6118, 35000 Rennes, France*
[b] *IPREM, UMR 5254, CNRS-Université de Pau et des Pays de L'Adour, 64000 Pau, France*
[c] *European Commission, Joint Research Centre (JRC), Directorate F - Health, Consumers and Reference Materials, Via E. Fermi 2749, 21027 Ispra, VA, Italy*
*\*julien.gigault@univ-rennes1.fr*

CRediT authorship contribution statement

- Alice Pradel: Conceptualization, Methodology, Investigation, Formal analysis, Writing - original draft, review & editing, Visualization.

- Hind el Hadri: Preparation of nanoplastic models.

- Cloé Desmet: Characterization of Particle Hydrophobicity.

- Jessica Ponti: Transmission Electron Microscopy Analysis.

- Stéphanie Reynaud: Preparation of nanoplastic models.

- Bruno Grassl: Conceptualization, Writing - review and editing.

- Julien Gigault: Conceptualization, Formal analysis, Writing - review and editing, Funding acquisition.

1    **Deposition of Environmentally Relevant Nanoplastic Models in Sand during Transport**

2    **Experiments**

3    Alice Pradel [a*], Hind el Hadri [b], Cloé Desmet[c], Jessica Ponti[c], Stéphanie Reynaud [b], Bruno Grassl [b],
4    Julien Gigault [a*]

5    *[a] Univ Rennes, CNRS, Géosciences Rennes - UMR 6118, 35000 Rennes, France*
6    *[b] IPREM, UMR 5254, CNRS-Université de Pau et des Pays de L'Adour, 64000 Pau, France*
7    *[c] European Commission, Joint Research Centre (JRC), Directorate F - Health, Consumers and*
8    *Reference Materials, Via E. Fermi 2749, 21027 Ispra, VA, Italy*
9    *[*]julien.gigault@univ-rennes1.fr*

10

11    **Abstract**

12    Nanoplastics (NPTs) are defined as colloids that originated from the unintentional degradation of

13    plastic debris. To understand the possible risks caused by NPTs, it is crucial to determine how they are

14    transported and where they may finally accumulate. Unfortunately, although most sources of plastic

15    are land-based, risk assessments concerning NPTs in the terrestrial environmental system (soils,

16    aquifers, freshwater sediments, etc.) have been largely lacking compared to studies concerning NPTs

17    in the marine system. Furthermore, an important limitation of environmental fate studies is that the

18    NPT models used are questionable in terms of their environmental representativeness. This study

19    describes the fate of different NPT models in a porous media under unfavorable (repulsive) conditions,

20    according to their physical and chemical properties: average hydrodynamic diameters (200 to 460 nm),

21    composition (polystyrene with additives or primary polystyrene) and shape (spherical or

22    polymorphic). NPTs that more closely mimic environmental NPTs present an inhomogeneous shape

23    (i.e., deviating from a sphere) and are more deposited in a sand column by an order of magnitude. This

24    deposition was attributed in part to physical retention, as confirmed by the straining that occurred for

25    the larger size fractions. Additionally, different Derjaguin-Landau-Verwey-Overbeek (DLVO) models

26    -the extended DLVO (XDLVO) and a DLVO modified by surface element integration (SEI) method-

27    suggest that the environmentally relevant NPT models may alter its orientation to diminish repulsion

28    from the sand surface and may find enough kinetic energy to deposit in the primary energetic

29    minimum. These results point to the importance of choosing environmentally relevant NPT models.

30    **Keywords**: Nanoplastic; Size; Shape; Transport; Soil; Column

31   **1. Introduction**:

32      It has been established that every environmental system contains plastic debris (Bank and

33   Hansson, 2019). The marine environment is the first system in which plastic pollution has been

34   extensively studied, probably due to the highly visible accumulation that started in the 1970s

35   (Carpenter and Smith, 1972; Cozar et al., 2014; Law et al., 2010; Schwarz et al., 2019). Since then, the

36   extent of this contamination has been more closely described. Plastic fragments or additives are found

37   in remote areas as they can travel long distances (Jamieson et al., 2017; Peng et al., 2020). They have

38   reached uninhabited forests after undergoing atmospheric transport (Allen et al., 2019) and have been

39   incorporated into Artic sea ice after being transported by oceanic currents (Obbard et al., 2014). It is

40   generally agreed upon that the terrestrial system is the major source of plastic waste (Jambeck et al.,

41   2015). However, plastics in terrestrial and freshwater environments have received little attention

42   (Horton et al., 2017; Rillig, 2012; Wagner et al., 2014). Plastic accumulates in the terrestrial system

43   due to common sources, such as faulty waste management systems, spreading of sewage sludge, use

44   of plastic mulches and other plastic products in agriculture, and tire wear particles (Carr et al., 2016;

45   He et al., 2018; Liu et al., 2019; Scheurer and Bigalke, 2018). This rapidly accumulating plastic in

46   soils and sediments can be degraded by photo-oxidation, thermo-oxidation, abrasion and

47   biodegradation, which causes the inevitable release of small plastic particles (Huerta Lwanga et al.,

48   2017; Ng et al., 2018). In the terrestrial system (soils, aquifers, sediments, etc.), studies have generally

49   focused on microplastics (1 μm to 5 mm) (Dong et al., 2019a, 2019b; He et al., 2018; Liu et al., 2019;

50   Tufenkji and Elimelech, 2005), although it is clear that plastic fragmentation does not stop at the

51   micrometer size (Gigault et al., 2016; Lambert and Wagner, 2016).

52      The fragmentation of macro- and microplastics to nanoplastics (<1 μm) adds complexity to the

53   global plastic waste issue. Even if no clear definition of nanoplastics (NPTs) is proposed by policy-

54   makers, a scientific consensus has been proposed to define NPTs as colloids that originate from the

55   unintentional degradation of plastic (Gigault et al., 2018; Hartmann et al., 2019). Compared to

56   microplastics, NPTs acquire colloidal properties and become unaffected by gravity. At this scale, the

57   fate of NPTs will be controlled by surface properties, shape and diffusion rather than by the bulk

2

58  properties (Hiemenz and Rajagopalan, 1997). The fact that the majority of plastic debris cannot be

59  located by mass budgets at the ocean surface suggests that part of the missing fraction of plastic debris

60  could be composed of fractions smaller than 300 µm in size (Albert A Koelmans et al., 2017; van

61  Sebille et al., 2015). Since the nanoscale characteristics of plastic debris may pose potential risks, it is

62  therefore crucial to determine where this plastic originates from and where it accumulates (Galloway,

63  2015; Albert A. Koelmans et al., 2017; Lehner et al., 2019).

64      Due to limited data on the occurrence of NPTs, lab-scale models can aid in determining the

65  transfer of NPTs from one environmental system to another. For the terrestrial system, a saturated

66  sand column is generally used as a proxy for the study of colloid transfer in soils, sediments and

67  aquifers (Geitner et al., 2017; Lecoanet et al., 2004; Petosa et al., 2010; Redman et al., 2004;

68  Syngouna and Chrysikopoulos, 2013; Tufenkji and Elimelech, 2004). Quevedo and Tufenkji

69  compared the transport of spherical and size standardized polystyrene nanoparticles in quartz sand and

70  loamy soil in the presence of monovalent or divalent salts (Quevedo and Tufenkji, 2012). Recently,

71  Hu et al. used quartz sand columns to investigate the cotransport of naphthalene with polystyrene

72  nanoparticles (Hu et al., 2020). Another recent work demonstrated the influence of the soil type on the

73  same nanoparticles (Wu et al., 2019). While these works highlight the importance and complexity of

74  the transport mechanisms in soils, they only focused on NPT models that are not representative of the

75  NPTs found in our environment (Ter Halle et al., 2017). Indeed, the composition, shape, size, and

76  surface are known to play key roles in the transport of nanoparticles in the environment (Hotze et al.,

77  2010; Pelley and Tufenkji, 2008; Salerno et al., 2006). Such parameters have only recently been

78  investigated, with studies concerning UV-aged NPTs (Liu et al., 2019) and polystyrene NPTs

79  containing different surface functionalities (Dong et al., 2019b).

80      Before investigating the influence of the soil properties, the objective of the present work is to

81  investigate how the properties of NPTs affect their transport or accumulation in soils. Thus, different

82  NPT models were used. All models were composed of polystyrene, since this is the only commercially

83  available nanometer-sized plastic particle available. On the one hand, both commercial and

84  noncommercial polystyrene latex spheres (PSL), *PSL COOH* and *PSL COOH-P,* respectively, are

85  synthesized by a bottom-up process (Pessoni et al., 2019). This makes them highly spherical and

86  monodisperse and it allows their surface to be modified by the addition of carboxylate functional

87  groups (COOH), which are common on weathered plastics (Gewert et al., 2015). On the other hand,

88  *NPT-P* are synthesized from a top-down method, which mimics the environmental mechanism of

89  abrasion (Hadri et al., 2020). They have polymorphic (asymmetrical & irregular) shapes, a

90  polydisperse size distribution, and they may contain some oxidized functional groups. The transport of

91  *NPT-P* models through a sand column shows that their irregular shape will increase their probability

92  of accumulating in porous media. These results stress the importance of choosing NPT models that

93  have environmentally relevant physicochemical properties.

94
95  **2.  Methods**

96  **2.1 Dispersions of nanoplastic models**

97  Table 1 presents the different NPT models used in the study.  Carboxylated polystyrene latex

98  spheres of 200 nm (*PSL COOH 200*) were Polybead® Carboxylate Orange Dyed Microspheres 0.20

99  μm purchased from (Polysciences© Warrington USA). These particles contain additives for stabilizing

100 purposes, whose composition and concentration are unknown. To study the effect of particle

101 composition, additive-free particles composed of primary (*-P*) polystyrene were also used. Soap and

102 metal-free carboxylated polystyrene spheres of 430 nm (*PSL COOH 430-P*) were produced by

103 emulsion polymerization according to the method described by Pessoni et al.(2019). Finally, NPT

104 models with polymorphic (asymmetrical and irregular)  shapes and with an average hydrodynamic

105 diameter of 350 nm or 460 nm (*NPT 350-P* and *NPT 460-P*, respectively) were formulated from

106 mechanically crushed PS pellets, according to the method previously described (Hadri et al., 2020).

107 All suspensions were composed of NaCl at a concentration of $5.0 \ 10^{-3}$ M with pH fixed at 6.5.

108   *Table 1: Summary of the physicochemical properties of the nanoplastic models studied*

| Model name | z-average diameter $d_{zH}$ (nm) | Polydispersity Index (PDI) | Area Equivalent Diameter (nm) | Aspect Ratio | Asperity Frequency ($nm^{-1}$) and *Amplitude (nm)* | Zeta potential (mV) | Particle Concentration ($\# L^{-1}$) |
|---|---|---|---|---|---|---|---|
| *PSL COOH 200* | $200 \pm 13$ | $0.04 \pm 0.03$ | $193 \pm 3$ | $1.01 \pm 0.01$ | 0 *0* | $-38.65 \pm 2.23$ | $1.14 \ 10^{12}$ |
| *PSL COOH 430-P* | $430 \pm 28$ | $0.07 \pm 0.01$ | $430 \pm 19$ | $1.01 \pm 0.01$ | 0.013 *12 ± 2* | $-29.07 \pm 1.81$ | $1.14 \ 10^{11}$ |
| *NPT 350-P* | $350 \pm 10$ | 0.11 | $244 \pm 133$ | $1.67 \pm 0.56$ | 0.013 *11 ± 6* | $-33.54 \pm 2.72$ | $2.12 \ 10^{11}$ |
| *NPT 460-P* | $460 \pm 25$ | 0.19 | $329 \pm 223$ | $1.68 \pm 0.58$ | | | $9.34 \ 10^{10}$ |

109

## 2.2 Charge characterization

111   The zeta potential of the particles was assessed using a Wallis zetameter by Cordouan

112   Technologies (Pessac, France). The particles were suspended in the same mobile phase as that used for

113   the experimental conditions: NaCl at $5.0 \ 10^{-3}$ M and pH 6.5. The electrophoretic mobility of the

114   colloidal particles was converted into a zeta potential by using Smoluchowski's formula. A zeta

115   potential for sand of -50 mV was chosen according to Vinogradov et al. (2010).

## 2.3 Size characterization

117   Hydrodynamic diameters ($d_H$) were determined by dynamic light scattering (DLS) using a

118   Vasco-Flex particle size analyzer (Cordouan Technologies). The $d_H$ of the injected NPT models and

119   the initial sand column signal, as well as 8 mL aliquots of the eluate, were characterized by DLS. Each

120   DLS measurement corresponds to an average of six measurements of 60 seconds ~~each~~. Each sample

121   was assigned a z-average hydrodynamic diameter ($d_{zH}$) using the cumulant algorithm. Additionally,

122   the Sparse Bayesian learning (SBL) algorithm provides a multimodal analysis to determine the

5

123    presence of several $d_H$ (see supplemental information, Figure S1). TEM images were obtained by a

124    Jeol 2100 High Resolution Microscope (Figure S2). Data was analyzed with ImageJ software and the

125    NanoDefine plugin  to obtain the area equivalent diameters and the aspect ratios (length of major

126    axis/length of minor axis), presented in Table 1 (Verleysen et al., 2019).

127

128    **2.4 Transport in porous media**

129    Transport and deposition were studied in a lab-scale sand-packed column using a liquid

130    chromatography system (Äkta™ Pure by General Electric Healthcare). This porous media was

131    composed of Fontainebleau sand (type NE34) with a median diameter ($d_{50}$) of 210 μm and a

132    uniformity index $d_{60}/d_{10}$ of 1.4. The sand was dry-packed into a borosilicate column (XK 26, GE

133    Healthcare, i.d. = 2.6 cm). The packed bed height varied from 11.2 to 12.7 cm. The porosity was 0.40

134    $\pm$ 0.01 on average. The eluent (mobile phase) was composed of NaCl at $5.0 \times 10^{-3}$ M. The pH value was

135    fixed at 6.5 using NaOH and HCl. The sand was washed with at least 14 pore volumes (PVs) of

136    deionized water and 22 PVs of the eluent. The pore volume was determined by an injection of NaCl at

137    $5.0 \times 10^{-3}$ M. Complete tracer tests were performed with KBr. All reactants were analytical grade. The

138    particles and tracers were injected during 6 PVs at a fixed rate of $1.57 \times 10^{-5}$ m.s$^{-1}$, followed by at least

139    six pore volumes of the plastic-free suspension at the same ionic strength and pH value.

140    At the outlet, the concentration of the NPT models eluted from the porous media was

141    continuously measured by the UV-Vis spectrophotometer paired to the chromatography system at a

142    wavelength $\lambda = 226$ nm, where polystyrene absorption is maximal. Breakthrough curves (BTC) were

143    obtained by plotting the outflowing concentration of the NPT models normalized by the initial

144    concentration as a function of pore volumes eluted. Duplicate experiments were performed for *PSL*

145    *COOH 200* and *PSL COOH 430-P*. Due to the limited yield of *NPT-P* dispersions and to the

146    variability in size distributions of different *NPT-P* batches, duplicates were not performed.

147

148     **2.5 Theory**

149         **2.5.1     Colloid Filtration Theory (CFT)**

150         Colloid filtration theory (CFT) is used to separate hydrodynamic processes from surface

151 interactions that are occurring in the sand column. It is summarized by equation (1), which expresses

152 the porous media's capacity to trap colloids. The single-collector removal efficiency ($\eta$) is the product

153 of the single-collector contact efficiency ($\eta_0$) and the attachment efficiency of the particles ($\alpha$) (Petosa

154 et al., 2010).

155 $$\eta = \eta_0\,\alpha \qquad\qquad\qquad (1)$$

156 The single-collector contact efficiency ($\eta_0$) is the capacity of colloids to be trapped by porous media

157 due only to hydrodynamic mechanisms, without any favorable physicochemical conditions. It depends

158 upon a number of factors, including the diameter of the colloids, the diameter of the sand grains in the

159 porous media, the porosity of the sand column, and the flow rate. It was calculated according to the

160 equation developed by Tufenkji and Elimelech (2004). The attachment efficiency ($\alpha$) is a function of

161 the physicochemical properties of the colloid dispersion and of the sand grain surfaces, such as ionic

162 strength, surface charge and the Hamaker constant of the system. The attachment efficiency (α) is

163 obtained according to equation (2):

164 $$\alpha = -\,\frac{2\,d_{50}}{3\,(1-\varepsilon)\eta_0 L}\ln(C/C_0) \qquad\qquad (2)$$

165 where $d_{50}$ is the median diameter of the sand grains, ε and L are the sand column porosity and length,

166 respectively, and ($C/C_0$) is the height of the breakthrough curve.

167         **2.5.1     DLVO theory of colloidal stability**

168         Surface energetics between particles and an infinite flat plane were modeled by the Derjaguin-

169 Landau-Verwey-Overbeek (DLVO) theory, such as the total energy of interaction $G^{tot}$ as the sum of

170 the Lifshitz-van der Waals $G^{LW}$ attraction and the repulsion due to the electronic double layer $G^{el}$.

171 DLVO theory can be expanded upon and modified to take into account the effect of hydrophobicity,

172 roughness and particle shape, separately. First an extended version of the DLVO theory (XDLVO)

173    was also modeled by adding the Lewis acid-base (hydrophopic) component G$^{AB}$ to the total energy of

174    interaction. Secondly, the effect of particle shape and orientation was studied thanks to the surface

175    element integration (SEI) method, since is what sets apart *PSL COOH 430-P* and both *NPT-P*

176    particles.

177    The Lifshitz–van der Waals component G$^{LW}$ of the free energy of interaction between a colloid and a

178    surface is given by:

179
$$G^{LW} = -\frac{H}{6}\left[\frac{2d_p(h+d_p)}{h(h+2d_p)} - Ln\frac{h+2d_p}{h}\right] \qquad (3)$$

180    where H is the Hamaker constant for the polystyrene-silica-water system, h is the separation distance

181    between the colloid and the sand, and $d_p$ is the radius of the colloid. A Hamaker constant of $1.45 \ 10^{-20}$

182    was calculated from Israelachvili (Israelachvili, 2015) for the interaction between quartz, water and

183    polystyrene.

184    The electronic double layer component G$^{el}$ is given by:

185
$$G^{el} = \pi\varepsilon d_p(\zeta_N^2 + \zeta_S^2)\left[\frac{2\zeta_N\zeta_S}{\zeta_N^2+\zeta_S^2}.Ln\frac{1+\exp(-\kappa h)}{1-\exp(-\kappa h)} + Ln\{1 - \exp(-2\kappa h)\}\right] \qquad (4)$$

186    where $\zeta_N$ and $\zeta_S$ are the surface charges of the plastic colloids and of the sand surface, respectively.

187    The zeta potential was used instead of the surface potential. $\kappa$ is the double layer thickness, which is

188    determined by the following equation:

189
$$\kappa = \left[\frac{e^2}{\varepsilon k_B T}\sum i z_i n_i\right]^2 \qquad (5)$$

190    where e is the charge of the electron; $\varepsilon$ is the permittivity of the medium, which is equal to $6.95 \ 10^{-10}$

191    $C^2.J^{-1}.m^{-1}$, $k_B$ the Boltzmann constant, T the temperature, $z_i$ the valency of the ions i, and $n_i$ the number

192    of ions i per unit volume.

193    The Lewis acid-base energy of interaction G$^{AB}$ of our system is:

194
$$G^{AB} = \pi r d_p \lambda \Delta G^{AB} e^{[(h_o-h)/\lambda]} \qquad (6)$$

8

195     where $\lambda$ is the correlation length, chosen as 1.65 nm, according to Valsesia et al. (2018), and $h_0$ is the

196     minimum distance of separation between the particle and the surface, taken as 0.158 nm. The acid-

197     base potential $\Delta G^{AB}$ is expressed as:

$$\Delta G^{AB} = -2\left(\sqrt{\gamma_N^{AB}} - \sqrt{\gamma_W^{AB}}\right) \cdot (\sqrt{\gamma_S^{AB}} - \sqrt{\gamma_W^{AB}})$$

198     with $\sqrt{\gamma^{AB}}$ referring to the polar component of the surface free energy for W = water, S = sand surface

199     and N = NPT model. $\sqrt{\gamma_W^{AB}}$ is 51.00 mJ.m$^{-2}$ and $\sqrt{\gamma_S^{AB}}$ is 15.00 mJ.m$^{-2}$ according to Barhoumi et al.

200     (Barhoumi et al., 2010).. The polar component of the free energy was measured according the method

201     of Valsesia et al. (2018) for each of the three types of NPT models. $\sqrt{\gamma_N^{AB}}$ values of 33.91, 37.47 and

202     31.82 mJ.m$^{-2}$ were obtained for *PSL COOH 200*, *PSL COOH 430-P* and *NPT-P*, respectively.

203        The DLVO theory was modified by the SEI method described by Wu et al. ( 2013) to understand

204     the effect of *NPT-P*'s nonspherical shape and their different orientations, described by the angle $\varphi$ that

205     is formed between the major axis of the particle and the collector surface (Bhattacharjee et al., 2000).

206     The interaction energy between a plane surface (collector) and a curved object (particle) were

207     calculated by integrating this energy over the exact surface geometry of the object. Our particles were

208     considered to be rod-like. The semi-major axis (L) and semi-minor axis (a) were determined according

209     to the aspect ratio and the $d_{zH}$ presented in Table 1.

210
211

### 3. Results & Discussion
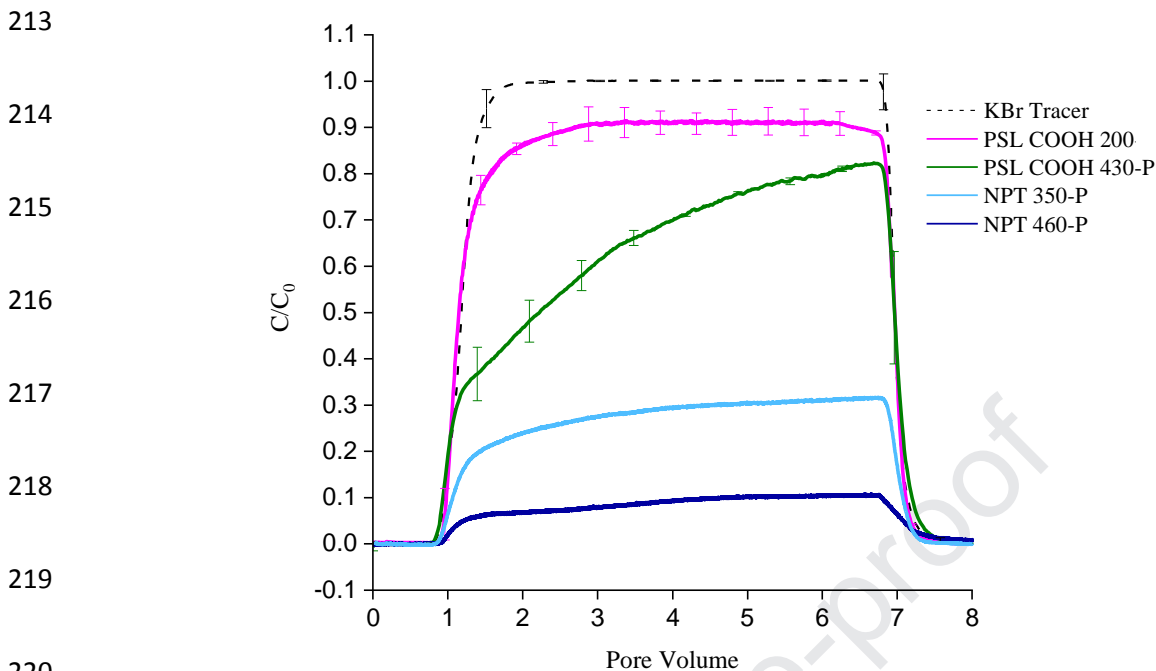


*Figure 1: Breakthrough curves of KCl tracer and nanoplastic models injected continuously for 6 pore volumes at an initial concentration ($C_0$) of $5.0 \ 10^{-3}$ g.$L^{-1}$ in $5.0 \ 10^{-3}$ M NaCl and pH 6.5 (error bars = standard deviation, n = 2).*

Figure 1 illustrates the breakthrough curves (BTC) of the different NPT models after transport through a sand column at a constant flow rate. Reproducible results are obtained with this experimental setup, as shown by the error bars on the duplicate experiments of *PSL COOH 200* and *PSL COOH 430-P*. A KBr salt tracer shows only the effect of transport by advection and dispersion due to the absence of deposition ($C/C_0$ of unity). *PSL COOH 200* presents a BTC similar in shape to KBr with 92±5% recovered in column effluent. This result indicates transport through the column with negligible deposition onto the sand. However, 67±1% of *PSL COOH 430-P* are recovered in column effluent, which indicates some deposition occurred. Finally, both polymorphic PS models (*NPT-P*) are the most deposited, with only 28% of *NPT 350-P*, and 10% of *NPT 460-P* that are recovered in column effluent. These results indicate that an increase in particle size causes an increase in the deposition rate. Indeed, when comparing NPT models of similar shape, larger particles are less recovered in column effluent: *PSL COOH 430-P* vs *PSL COOH 200* and *NPT 460-P* vs *NPT 350-P*. The higher transport rate of *PSL COOH 200* compared to *PSL COOH 430-P* may also be due to the

10

236 presence of surfactants used for commercial *PSL COOH-200*. Such molecules can enhance

237 nanoparticle transport by decreasing adsorption in the secondary energetic minimum (see DLVO

238 section below) (Tufenkji and Elimelech, 2005). Finally, the absence of a tailing at the end of the BTCs

239 shows that deposited particles did not detach from the porous media (Bradford et al., 2002).

240 Based on the BTCs, it appears that the particle shape strongly increases the deposition rate in

241 the porous media under dynamic conditions. Surprisingly, *NPT 350-P* is significantly more deposited

242 in porous media than *PSL COOH 430-P,* although they have a smaller initial hydrodynamic diameter

243 and area equivalent diameter (Table 1). This confirms that the asymmetrical and irregular shape of the

244 NPT model (*NPT-P*) significantly increases deposition in the porous media. It should be noted that

245 these experiments were performed at equivalent mass concentrations instead of equivalent particle

246 concentrations. This method was chosen to obtain a quality DLS signal at the outlet of the sand

247 column since light scattering is proportional to the particle diameter. However, it creates a bias that

248 favors elution of the smaller, more numerous particles (Table 1) (Bradford and Bettahar, 2006).

249 Despite this, *NPT 350-P*, which has a higher particle concentration, was more deposited than *PSL*

250 *COOH 430-P*. This highlights the fact that an irregular asymmetrical shape has a greater impact on the

251 deposition rate than that of size and particle concentration.

252 To investigate the retention mechanisms of these NPT models, both colloidal filtration theory

253 (CFT) and various Derjaguin-Landau-Verwey-Overbeek (DLVO) theories were studied. According to

254 the CFT, the single-collector contact efficiency ($\eta_0$) increases as sub-micrometric particle sizes

255 decrease (Tufenkji and Elimelech, 2004). Hence, smaller particles should be more easily retained,

256 which is not the case in the present study. This suggests that nanoplastic models used here have

257 considerable differences in attachment efficiency ($\alpha$) and non-classical mechanisms of particle

258 collision are operating. The attachment efficiency ($\alpha$) obtained by CFT, can be used to compare the

259 affinity of particles with sand across different experimental conditions. Caution must be taken in

260 interpreting $\alpha$ since the CFT is meant to study monodisperse and spherical particles and collectors.

261 Since the sand grains are not monodisperse ($d_{60}/d_{10}$ of 1.4) and nanoplastic models have different

262 degrees of polydispersity (see Table 1), an average $\alpha$ range, named $\bar{\alpha}$, and a range of $\alpha$ were presented

263   in Table 2 with the corresponding heat-maps presented in supplementary information (Figure S3).

264   An $\bar{\alpha}$ of 0.0034 ± 0.0005 was obtained for *PSL COOH 200,* whereas *PSL COOH 430-P* had an $\bar{\alpha}$ =

265   0.012 ± 0.0008 (Table 2). These results are in agreement with other studies, such as Bradford et al.

266   (2002), who found that the 450 nm carboxylated PSL attachment efficiency in $10^{-3}$ M KCl at pH 6.8

267   varied from $\alpha$ = 0.0037 to $\alpha$ = 0.014 according to the polydispersity and average grain size of the

268   quartz sand (Bradford et al., 2002). Tufenkji and Elimelech (2005) found $\alpha$ values of 0.0058 and 0.014

269   for 320 nm PSL COOH in 20 $10^{-3}$ M KCl at pH 8. For the polymorphic NPT models, the average

270   attachment efficiency is one order of magnitude greater than that for the spherical models, with $\alpha$ =

271   0.069 for *NPT 350-P* and 0.14 for *NPT 460-P*. This large increase in attachment efficiency is more

272   likely to represent different hydrodynamic flow processes than a change in surface affinity. Indeed, the

273   CFT theory is unsuitable to study the flow of nonspherical particles and largely overestimates $\alpha$ (and

274   underestimates $\eta_0$) when the particle shape deviates from that of a sphere (Salerno et al., 2006).

275   *Table 2: Summary of the percent in column effluent and attachment efficiencies (α) for the different nanoplastic models. The*

276   *attachment efficiencies are based on average particle diameter ($d_p$) and collector diameters ($d_c$) and a range of dp and dc*

277   *equal to the standard deviation (σ) of the size distributions. (Error bars = standard deviation of the duplicate experiments).*

| Nanoplastic Model | Percent in Column Effluent (%) | Attachment Efficiency ($\alpha$) | | |
|---|---|---|---|---|
| | | dp – $\sigma$ and dc - $\sigma$ | Average dp and dc | dp + $\sigma$ and dc + $\sigma$ |
| *PSL COOH 200* | 92 ± 5 | $2.0 \ 10^{-3} \pm 0.4 \ 10^{-3}$ | $3.4 \ 10^{-3} \pm 0.5 \ 10^{-3}$ | $5.4 \ 10^{-3} \pm 1.1 \ 10^{-3}$ |
| *PSL COOH 430-P* | 67 ± 1 | $6.9 \ 10^{-3} \pm 0.8 \ 10^{-3}$ | $1.2 \ 10^{-2} \pm 0.1 \ 10^{-2}$ | $1.9 \ 10^{-2} \pm 0.2 \ 10^{-2}$ |
| *NPT 350-P* | 28 | $4.0 \ 10^{-2}$ | $6.9 \ 10^{-2}$ | $1.2 \ 10^{-1}$ |
| *NPT 460-P* | 10 | $7.9 \ 10^{-2}$ | $1.4 \ 10^{-1}$ | $2.5 \ 10^{-1}$ |

278

279       Since the attachment efficiencies ($\alpha$) obtained by the CFT theory should only reflect surface

280   energetic interactions, they can be compared with the profiles of the interaction energy between the

281   particles and the sand. Total surface energetic interactions ($G^{tot}$) are modeled according to DLVO

282   theory by taking the sum of the Lifshitz-van der Waals attraction ($G^{LW}$) and the repulsion due to the

283      electronic double layer ($G^{el}$). An extended version, the XDLVO theory, includes the Lewis acid-base

284      (hydrophobic) interaction energy ($G^{AB}$). This component has been carefully quantified using the

285      method described by Valsesia et al. (2018). It should be noted, however, that since DLVO and

286      XDLVO theories assume that the particles are spherical, they cannot correctly determine the

287      interaction energy of the asymmetrical and irregularly shaped *NPT-P*s (Hotze et al., 2010). To

288      overcome this limitation, a SEI-modified DLVO calculates $G^{LW}$ and $G^{el}$ between an elongated particle

289      and the sand surface. This modified DLVO does not, however, incorporate the hydrophobic

290      component of the interaction energy. It is important to note that in these experimental conditions,

291      advection prevails over diffusion, with a Peclet number varying from 112 to 240 for *PSL COOH 200*

292      and *NPT 460-P*, respectively. In these conditions, particle deposition can occur if the adhesive forces

293      are stronger than the hydrodynamic forces. Therefore, the objective is only to investigate whether the

294      physical and chemical properties of the particles modeled by the different DLVO theories, are

295      correlated to the attachment efficiencies in the sand column and hence a good predictor of adhesive

296      forces. Surface energetic interactions should not be considered an absolute prediction of deposition

297      behavior. If the energy of interaction predicts trends in transport, the most transported particles should

298      have the highest energetic barrier to deposition ($\Delta G^{tot}_{max}$) and lowest secondary energetic minimum

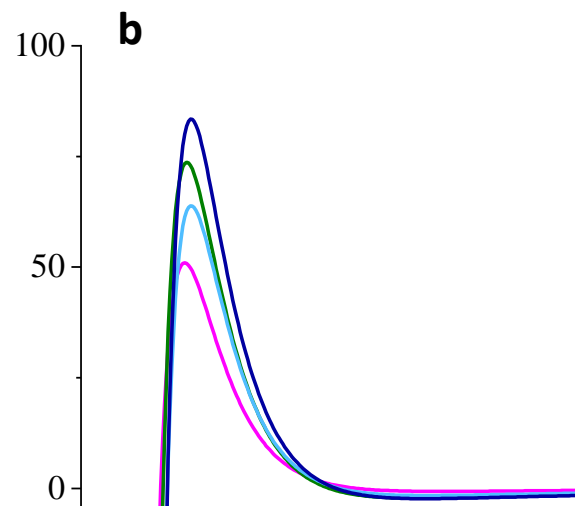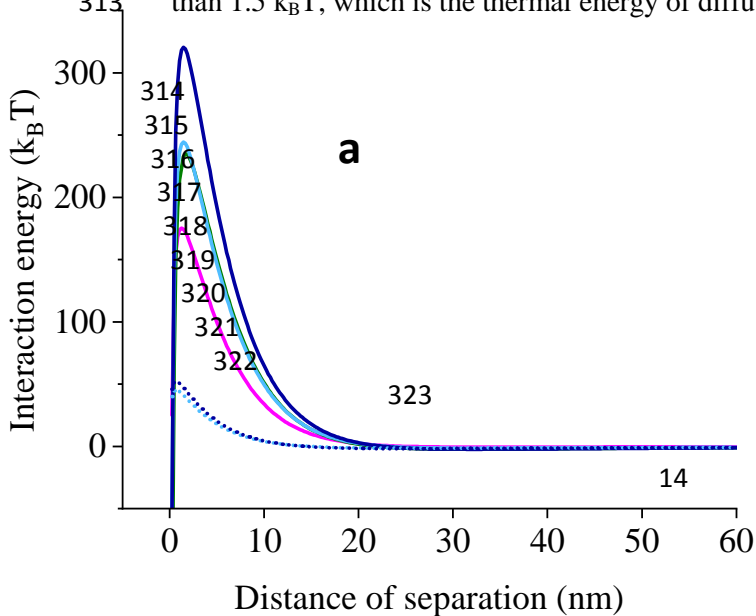299      ($\Delta G^{tot}_{min2}$), where reversible deposition can occur.

300

301

302 *Table 3: Summary of primary maximum (ΔG$^{tot}_{max}$) and secondary energetic minimum (ΔG$^{tot}_{min2}$) of interaction energies*

303 *according to DLVO, SEI -modified DLVO and XDLVO theories, for the different nanoplastic models.*

| | DLVO Theory | | SEI-modified DLVO Theory | | | | XDLVO Theory | |
| | | | $\varphi$ = 0 radians | | $\varphi$ = $\pi$/3 radians | | | |
| Nanoplastic Model | ΔG$^{tot}_{max}$ (k$_B$T) | ΔG$^{tot}_{min2}$ (k$_B$T) | ΔG$^{tot}_{max}$ (k$_B$T) | ΔG$^{tot}_{min2}$ (k$_B$T) | ΔG$^{tot}_{max}$ (k$_B$T) | ΔG$^{tot}_{min2}$ (k$_B$T) | ΔG$^{tot}_{max}$ (k$_B$T) | ΔG$^{tot}_{min2}$ (k$_B$T) |
|---|---|---|---|---|---|---|---|---|
| *PSL COOH 200* | 175 | -0.7 | - | - | - | - | 51 | -0.7 |
| *PSL COOH 430-P* | 235 | -2.2 | - | - | - | - | 74 | -2.0 |
| *NPT 350-P* | 244 | -1.6 | 4.5 10$^{10}$ | -0.4 | 45 | -1.5 | 64 | -1.6 |
| *NPT 460-P* | 321 | -2.3 | 5.9 10$^{10}$ | -0.4 | 52 | -1.8 | 83 | -2.3 |

304

305    According to DLVO theory, all particles undergo significant repulsion from the sand grains,

306 with ΔG$^{tot}_{max}$ equal to 175 k$_B$T for *PSL COOH 200,* 235 k$_B$T for *PSL COOH 430-P*, 244 k$_B$T for *NPT*

307 *350-P,* and 321 k$_B$T for *NPT 460-P* (Table 3 and full lines in Figure 2a). Based on the energy profiles,

308 no colloid can overcome the energy barrier (ΔG$^{tot}_{max}$) and irreversibly deposit in the primary minimum

309 (ΔG$^{tot}_{min1}$). The secondary energetic minimum (ΔG$^{tot}_{min2}$) occurs between 20 and 60 nm from the sand

310 surface. It varies from as low as -2.3 k$_B$T for *NPT 460-P,* -2.2 k$_B$T for *PSL COOH 430-P*, -1.6 k$_B$T for

311 *NPT 460-P* to -0.7 k$_B$T for *PSL COOH 200* (Table 3 and full lines in Figure 2c). For the three larger

312 particles, reversible retention in the secondary energetic minimum can occur since the depth is larger
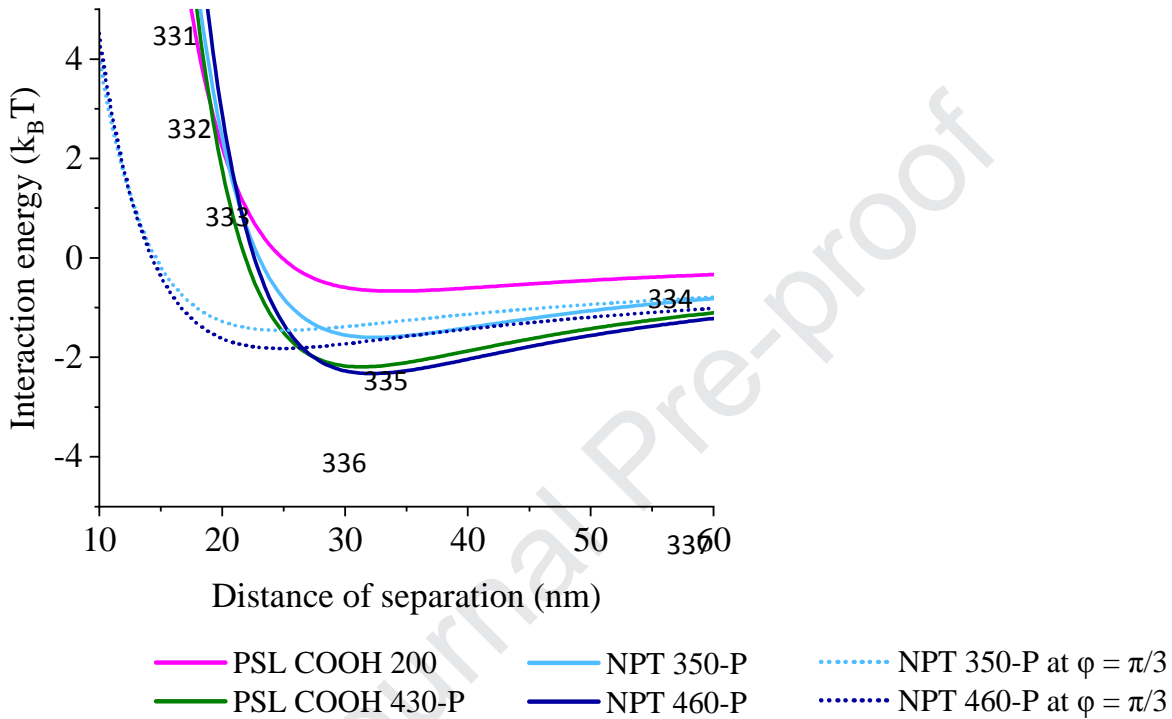
313    than 1.5 k$_B$T, which is the thermal energy of diffusion (Israelachvili, 2015).

324
325
326
327
328

329

330



338

PSL COOH 200 —— NPT 350-P ······· NPT 350-P at $\varphi = \pi/3$

339 PSL COOH 430-P —— NPT 460-P ······· NPT 460-P at $\varphi = \pi/3$

340 *Figure 2: Interaction energy, scaled to $k_BT$, between the nanoplastic models and the sand grain collector as a function of*

341 *distance according to a) DLVO theory (full lines) and SEI -modified DLVO theory (dashed lines) and b) XDLVO theory. The*

342 *identical data is replotted in c) and d) to highlight the secondary energetic minimum of panels a) and b) respectively.*

343

344    By accounting for the polar component of the interaction energy, the XDLVO theory predicts

345 similar global trends but indicates a much lower repulsion of all particles from the sand surface

346 (Figures 2b and 2d). The maximum heights of $\Delta G^{tot}_{max}$ for spherical particles *PSL COOH 200* and *PSL*

347 *COOH 430-P* are equal to 51 $k_BT$ and 74 $k_BT$, respectively. For the asymmetrical and irregularly

348 shaped particles, $\Delta G^{tot}_{max}$ is comparable: 64 $k_BT$ and 83 $k_BT$ for *NPT 350-P* and *NPT 460-P*,

349 respectively (Table 3 and Figure 2b). Based on the height of the energy barriers, still no colloid

15

350 deposition should occur in the primary minima. The depth of the secondary energetic minimum

351 ($\Delta G^{tot}_{min2}$) is unchanged compared to that determined by the DLVO theory (Table 3 and Figure 2d).

352       The dashed lines in Figures 2a and 2c show the minimal interaction energy between the sand

353 surface and the *NPT-P* models, according to the SEI-modified DLVO theory. This occurs when they

354 form an angle ($\varphi$) of $\pi/3$ with the collector surface (Gomez-Flores et al., 2019). $\Delta G^{tot}_{max}$ is reduced to

355 45 $k_BT$ and 52 $k_BT$ for *NPT 350-P* and *NPT 460-P*, respectively (Table 3). The interaction energy is

356 maximal at $\varphi = 0$ (Table 3 and Figure S4). This is mostly due to the fact the particle surface is closer to

357 the collector (Gomez-Flores et al., 2019). $\Delta G^{tot}_{min2}$ is only slightly less deep than predicted by DLVO

358 and XDLVO theories (Table 3 and Figure 2c).

359       The high retention rate of the *NPT-P* particles can be in part attributed to the fact that they

360 may find orientations where there is no energy barrier to irreversible deposition ($\Delta G^{tot}_{min1}$) (Gomez-

361 Flores et al., 2019). This can be expected to occur when both particle orientation and hydrophobicity

362 are accounted for simultaneously. Furthermore, the magnitude of the total energies of interaction

363 ($\Delta G^{tot}$) of *PSL COOH 430-P, NPT 350-P* and *NPT 460-P*s and the sand surfaces may be overestimated

364 by the all DLVO models due to their surface roughness (Table 1 and Figure S2) (Bhattacharjee et al.,

365 1998; Hoek and Agarwal, 2006). *NPT-P* particles are characterized by a large range of orientation-

366 dependent interaction energies (Table 3 and S5), which will give them considerable torque. This added

367 torque can provide the particles sufficient kinetic energy to overcome an energy barrier ($\Delta G^{tot}_{max}$) that

368 is significantly reduced at some orientations Figure 2a (Seymour et al., 2013).

369       However, the DLVO and XDLVO theories are inadequate to predict the deposition of plastic

370 nanoparticles in porous media. On the one hand, the DLVO and XDLVO theories globally

371 underestimate the amount of deposition that particles undergo. This is a well-known effect when

372 studying the transport of particles in unfavorable (repulsive) conditions (Elimelech and O'Melia,

373 1990). On the other hand, the height of the energy barrier is not proportional to the level of repulsion,

374 nor is the depth of the secondary energetic minimum proportional to the level of deposition. For

375 example, *PSL COOH 200* is the most transported particle, although it has the lowest energy barrier

376 ($\Delta G^{tot}_{max}$). This occurs because all interaction energies scale linearly with particle size (Elimelech and

377  O'Melia, 1990). In other words, larger particles should undergo more repulsion and be more

378  transported, especially since all particles present comparable polar components of the surface free

379  energy ($\gamma^{AB}$) and zeta potentials ($\zeta_N$). However, contrary to these DLVO and XDLVO predictions,

380  *NPT 460-P*, which has a higher energy barrier, is more deposited than *NPT 350-P*. Although a high

381  energy barrier is present, particles may be retained by 1) attachment onto chemical heterogeneities on

382  the colloid and collector surfaces that act as favorable sites (Seymour et al., 2013; Tufenkji and

383  Elimelech, 2005) 2) reversible attachment in the secondary energetic minimum (Tufenkji and

384  Elimelech, 2005) and 3) straining (trapping of particles in pore throats that are too small to allow the

385  passage of particles) (Bradford et al., 2002; McDowell-Boyer et al., 1986). Furthermore, pore

386  geometry creates a variety of speed profiles, such that particles may also be retained in zones with a

387  lower flow velocity where the hydrodynamic forces are lowered (Elimelech and O'Melia, 1990).

388  Indeed, pore geometry plays a dominant role in colloid retention under conditions where a high energy

389  barrier exists (Tong and Johnson, 2006).

390       To determine the extent to which deposition can be attributed to chemical heterogeneity, batch

391  adsorption experiments were conducted. The results, presented in S5, show that none of our plastic

392  nanoparticles are significantly adsorbed onto the sand. While results from batch and column

393  experiments can be difficult to compare when they are not normalized by $\bar{\alpha} = 1$, our batch experiments

394  do show that chemical heterogeneity is far from significative (Geitner et al., 2017; Treumann et al.,

395  2014). This points to the importance of straining and adsorption in the secondary energetic minimum.
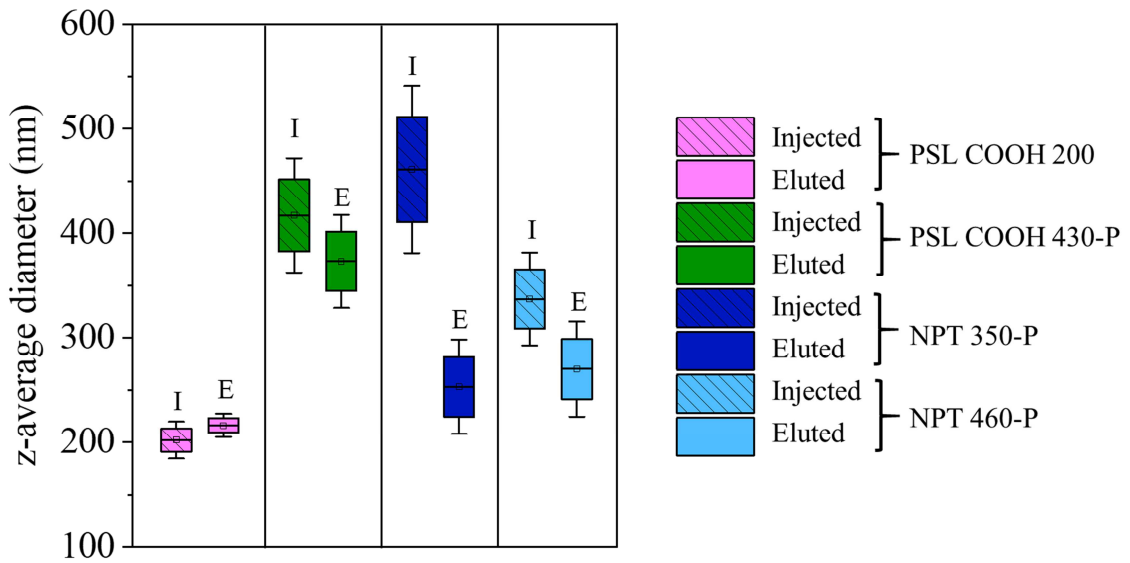
397    *Figure 3: z-average hydrodynamic diameters ($d_{zH}$) of the plastic nanoparticles before and after flowing through the sand*

398    *column (n=6, error bars= standard deviation).*

399    The evolution of the hydrodynamic diameters of the particles injected in and eluted from

400    through the porous media can also indicate what processes occur in the column (Figure 3). The

401    average size and polydispersity of eluted particles were constant during elution. The average

402    hydrodynamic diameters ($d_{zH}$) of the smaller spheres, *PSL COOH 200*, do not change significantly

403    (+4%). The larger spherical particles, *PSL COOH 430-P,* undergo a more pronounced decrease in $d_{zH}$

404    after flowing through the sand column (-11%). Both spherical particles' polydispersities do not vary

405    significantly. For the asymmetrical NPT models, the decrease in $d_{zH}$ after elution is globally greater

406    and even more pronounced for the larger particles (-45% for *NPT 460-P*) compared to that of the

407    smaller                                                                                            particles

408    (-20% for *NPT 350-P*). The smaller size fraction of irregularly shaped particles, approximately 200 nm

409    in diameter, is most mobile in the sand column. Furthermore, the polydispersity of the samples

410    containing asymmetrical and irregular particles decreases. These changes in size point to a mechanism

411    of physical retention of spherical particles larger than 380 nm and irregularly shaped particles larger

412    than approximately 200 nm. This confirms that large particles are deposited by physical straining in

413    the pores of the sand column, which is unaccounted for by the DLVO theories and underestimated by

414 CFT (Bradford et al., 2002). In similar experimental conditions, Weiss et al. (Weiss et al., 1995) noted

415 a similar effect concerning the transport of 14 different bacterial strains. The bacterial cells recovered

416 in the eluent were not only smaller but also rounder than the cells injected.

417       The deposition rate increases as the particle size increases and as its shape deviates from that

418 of a sphere. In other words, smaller and smoother particles are more easily transported. This can be

419 partially attributed to straining. Straining is expected to start having an effect when the ratio of the

420 particle radius to the median collector radius ($d_p/d_{50}$) exceeds 0.0017 (Bradford et al., 2002). This is

421 satisfied in the case of *PSL COOH 430-P* ($d_p/d_{50}$ = 0.002). Concerning *NPT-Ps*, since most particles

422 larger than approximately 200 nm are retained, straining occurs at a lower $d_p/d_{50}$ ratio (Figure 3).

423 Straining of these particles is enhanced because the hydrodynamics of nonspherical particle flow in

424 porous media are more complex than those of spherical particles. In highly repulsive conditions

425 (thousands of $k_BT$), elongated particles and are not more deposited than spherical particles since they

426 can orient their major axis parallel to the flow (Xu et al., 2008). However, in our conditions, where

427 there is less repulsion (10s of $k_BT$) nonspherical particles are increasingly deposited. This is attributed

428 to larger collision frequencies with the porous media (Salerno et al., 2006). The CFT underestimates

429 the single-collector contact efficiency ($\eta_0$) for spheroidal particles (Salerno et al., 2006). Finally, the

430 *NPT-P* dispersions are highly polydisperse and as such will contain a higher fraction of large particles

431 that are likely to be retained.

432       As mentioned above, reversible deposition in the secondary energetic minimum is possible for

433 *PSL COOH 430-P* and both polymorphic particles *NPT 350-P* and *NPT 460-P*. The asymmetrical

434 BTC shape of the *PSL COOH 430-P* is typical of either particle release from the secondary energetic

435 minimum or blocking of the flowing particles by previously deposited particles (Bradford et al., 2002;

436 Bradford and Bettahar, 2006; Redman et al., 2004; Tufenkji and Elimelech, 2005). This was not

437 observed for *NPT 350-P* and *NPT 460-P*, whose BTCs instead reach a plateau. It indicates either that

438 the asymmetrical models are not detached and undergoing re-entrainment from the sand or that

439 deposited particles do not block the incoming particles. Colloidal detachment and re-entrainment from

440 the secondary energetic minimum mostly occur by rolling, which is easiest for spherical particles.

441    Despite the fact that nonspherical particles have larger hydrodynamic torques than spherical particles,

442    as particles deviate from an ideal spherical shape, they present a higher moment arm requiring more

443    energy to induce rolling (Bergendahl and Grasso, 2000; Seymour et al., 2013) The flat BTC may also

444    indicate that deposited particles create more favorable sites for deposition by increasing the physical

445    roughness of the porous media (Seymour et al., 2013). Finally, the shape of the *NPT-P*'s BTCs

446    suggest that reversible deposition not be as dominant a mechanism as straining and deposition in the

447    primary energetic minimum.

448    **4. Conclusion**

449    This study showed that the physicochemical properties of the NPT models significantly affect

450    their propensity to be transported. The asymmetrical and irregular shape of the environmentally

451    relevant NPT model has a strikingly positive impact on the deposition rate in the sand column

452    compared to that impact of particle size, composition or concentration. The deposition of these models

453    in the porous media may be attributed partially to physical retention, as witnessed by the straining of

454    the larger size fractions. Their deposition is also attributed to an orientation-dependent level of

455    repulsion ($\Delta G^{tot}_{max}$) which allows the particles to take on the most thermodynamically preferable

456    orientation, and possibly to overcome the energy barrier to irreversible deposition ($\Delta G^{tot}_{max}$), given

457    sufficient hydodynamic torque. These results point to the importance of choosing environmentally

458    relevant NPT models. Their asymmetrical and irregular shape, which is characteristic of the

459    mechanical abrasion of plastic debris, increases their deposition rate in a sand column by an order of

460    magnitude. It is clear that the relevance of environmental fate studies depends upon the quality of the

461    proxies used (Koelmans, 2019). More particularly, the impact of the NPT composition (polymer type,

462    additives and sorbed contaminants), average size and size distribution as well as NPT shape are crucial

463    parameters to study (Wagner and Reemtsma, 2019).

464    The importance of the physical and chemical properties of the NPT models has been

465    demonstrated here. Further studies are needed on the one hand, to define single-collector contact

466    efficiency ($\eta_0$) for nonspherical particles and to quantify the amount of deposition that can be

467    attributed to straining, irreversible attachment (in $\Delta G^{tot}_{min1}$) and reversible attachment (in $\Delta G^{tot}_{min2}$). On

468 the other hand, more research is needed to implement these results by taking into account the

469 environmental conditions of the porous media (ionic strength, natural organic matter, pH value, and

470 soil composition). Such a complete approach is needed to fully assess the fate of NPTs in freshwater

471 and terrestrial environments.

472

473 **Competing Interest Statement**

474 The authors declare that they have no competing interests.

475 **References**

476 Allen, S., Allen, D., Phoenix, V.R., Le Roux, G., Durántez Jiménez, P., Simonneau, A., Binet, S., Galop,
477        D., 2019. Atmospheric transport and deposition of microplastics in a remote mountain
478        catchment. Nature Geoscience. https://doi.org/10.1038/s41561-019-0335-5
479 Bank, M.S., Hansson, S.V., 2019. The Plastic Cycle: A Novel and Holistic Paradigm for the
480        Anthropocene. Environ. Sci. Technol. acs.est.9b02942.
481        https://doi.org/10.1021/acs.est.9b02942
482 Barhoumi, H., Maaref, A., Jaffrezic-Renault, N., 2010. Experimental Study of Thermodynamic Surface
483        Characteristics and pH Sensitivity of Silicon Dioxide and Silicon Nitride. Langmuir 26, 7165–
484        7173. https://doi.org/10.1021/la904251m
485 Bergendahl, J., Grasso, D., 2000. Prediction of colloid detachment in a model porous media:
486        hydrodynamics. Chemical Engineering Science 55, 1523–1532.
487        https://doi.org/10.1016/S0009-2509(99)00422-4
488 Bhattacharjee, S., Chen, J.Y., Elimelech, M., 2000. DLVO interaction energy between spheroidal
489        particles and a flat surface. Colloids and Surfaces A: Physicochemical and Engineering Aspects
490        165, 143–156. https://doi.org/10.1016/S0927-7757(99)00448-3
491 Bhattacharjee, S., Ko, C.-H., Elimelech, M., 1998. DLVO Interaction between Rough Surfaces.
492        Langmuir 14, 3365–3375. https://doi.org/10.1021/la971360b
493 Bradford, S.A., Bettahar, M., 2006. Concentration dependent transport of colloids in saturated
494        porous media. Journal of Contaminant Hydrology 82, 99–117.
495        https://doi.org/10.1016/j.jconhyd.2005.09.006
496 Bradford, S.A., Yates, S.R., Bettahar, M., Simunek, J., 2002. Physical factors affecting the transport
497        and fate of colloids in saturated porous media: FACTORS AFFECTING THE FATE OF COLLOIDS.
498        Water Resources Research 38, 63-1-63–12. https://doi.org/10.1029/2002WR001340
499 Carpenter, E.J., Smith, K.L., 1972. Plastics on the Sargasso Sea Surface. Science 175, 1240–1241.
500        https://doi.org/10.1126/science.175.4027.1240
501 Carr, S.A., Liu, J., Tesoro, A.G., 2016. Transport and fate of microplastic particles in wastewater
502        treatment plants. Water Research 91, 174–182.
503        https://doi.org/10.1016/j.watres.2016.01.002
504 Cozar, A., Echevarria, F., Gonzalez-Gordillo, J.I., Irigoien, X., Ubeda, B., Hernandez-Leon, S., Palma,
505        A.T., Navarro, S., Garcia-de-Lomas, J., Ruiz, A., Fernandez-de-Puelles, M.L., Duarte, C.M.,
506        2014. Plastic debris in the open ocean. Proceedings of the National Academy of Sciences 111,
507        10239–10244. https://doi.org/10.1073/pnas.1314705111
508 Dong, Z., Zhang, W., Qiu, Y., Yang, Z., Wang, J., Zhang, Y., 2019a. Cotransport of nanoplastics (NPs)
509        with fullerene (C60) in saturated sand: Effect of NPs/C60 ratio and seawater salinity. Water
510        Research 148, 469–478. https://doi.org/10.1016/j.watres.2018.10.071

511 Dong, Z., Zhu, L., Zhang, W., Huang, R., Lv, X., Jing, X., Yang, Z., Wang, J., Qiu, Y., 2019b. Role of
512        surface functionalities of nanoplastics on their transport in seawater-saturated sea sand.
513        Environmental Pollution 255, 113177. https://doi.org/10.1016/j.envpol.2019.113177

514 Elimelech, M., O'Melia, C.R., 1990. Effect of particle size on collision efficiency in the deposition of
515        Brownian particles with electrostatic energy barriers. Langmuir 6, 1153–1163.
516        https://doi.org/10.1021/la00096a023

517 Galloway, T.S., 2015. Micro- and Nano-plastics and Human Health, in: Bergmann, M., Gutow, L.,
518        Klages, M. (Eds.), Marine Anthropogenic Litter. Springer International Publishing, Cham, pp.
519        343–366. https://doi.org/10.1007/978-3-319-16510-3_13

520 Geitner, N.K., O'Brien, N.J., Turner, A.A., Cummins, E.J., Wiesner, M.R., 2017. Measuring Nanoparticle
521        Attachment Efficiency in Complex Systems. Environmental Science & Technology 51, 13288–
522        13294. https://doi.org/10.1021/acs.est.7b04612

523 Gewert, B., Plassmann, M.M., MacLeod, M., 2015. Pathways for degradation of plastic polymers
524        floating in the marine environment. Environmental Science: Processes & Impacts 17, 1513–
525        1521. https://doi.org/10.1039/C5EM00207A

526 Gigault, J., Halle, A. ter, Baudrimont, M., Pascal, P.-Y., Gauffre, F., Phi, T.-L., El Hadri, H., Grassl, B.,
527        Reynaud, S., 2018. Current opinion: What is a nanoplastic? Environmental Pollution 235,
528        1030–1034. https://doi.org/10.1016/j.envpol.2018.01.024

529 Gigault, J., Pedrono, B., Maxit, B., Halle, A.T., 2016. Marine plastic litter: the unanalyzed nano-
530        fraction. Environ. Sci.: Nano 3, 346–350. https://doi.org/10.1039/C6EN00008H

531 Gomez-Flores, A., Bradford, S.A., Wu, L., Kim, H., 2019. Interaction energies for hollow and solid
532        cylinders: Role of aspect ratio and particle orientation. Colloids and Surfaces A:
533        Physicochemical and Engineering Aspects 580, 123781.
534        https://doi.org/10.1016/j.colsurfa.2019.123781

535 Hadri, H.E., Gigault, J., Maxit, B., Grassl, B., Reynaud, S., 2020. Nanoplastic from mechanically
536        degraded primary and secondary microplastics for environmental assessments. NanoImpact
537        100206. https://doi.org/10.1016/j.impact.2019.100206

538 Hartmann, N.B., Hüffer, T., Thompson, R.C., Hassellöv, M., Verschoor, A., Daugaard, A.E., Rist, S.,
539        Karlsson, T., Brennholt, N., Cole, M., Herrling, M.P., Hess, M.C., Ivleva, N.P., Lusher, A.L.,
540        Wagner, M., 2019. Are We Speaking the Same Language? Recommendations for a Definition
541        and Categorization Framework for Plastic Debris. Environ. Sci. Technol. 53, 1039–1047.
542        https://doi.org/10.1021/acs.est.8b05297

543 He, L., Wu, D., Rong, H., Li, M., Tong, M., Kim, H., 2018. Influence of Nano- and Microplastic Particles
544        on the Transport and Deposition Behaviors of Bacteria in Quartz Sand. Environ. Sci. Technol.
545        acs.est.8b01673. https://doi.org/10.1021/acs.est.8b01673

546 Hiemenz, P.C., Rajagopalan, Raj., 1997. Principles of colloid and surface chemistry. Dekker, New York;
547        Basel; Hong Kong.

548 Hoek, E.M.V., Agarwal, G.K., 2006. Extended DLVO interactions between spherical particles and
549        rough surfaces. Journal of Colloid and Interface Science 298, 50–58.
550        https://doi.org/10.1016/j.jcis.2005.12.031

551 Horton, A.A., Walton, A., Spurgeon, D.J., Lahive, E., Svendsen, C., 2017. Microplastics in freshwater
552        and terrestrial environments: Evaluating the current understanding to identify the
553        knowledge gaps and future research priorities. Science of The Total Environment 586, 127–
554        141. https://doi.org/10.1016/j.scitotenv.2017.01.190

555 Hotze, E.M., Phenrat, T., Lowry, G.V., 2010. Nanoparticle Aggregation: Challenges to Understanding
556        Transport and Reactivity in the Environment. Journal of Environment Quality 39, 1909.
557        https://doi.org/10.2134/jeq2009.0462

558 Hu, E., Shang, S., Fu, Z., Zhao, X., Nan, X., Du, Y., Chen, X., 2020. Cotransport of naphthalene with
559        polystyrene nanoplastics (PSNP) in saturated porous media: Effects of PSNP/naphthalene
560        ratio and ionic strength. Chemosphere 245, 125602.
561        https://doi.org/10.1016/j.chemosphere.2019.125602

562     Huerta Lwanga, E., Mendoza Vega, J., Ku Quej, V., Chi, J. de los A., Sanchez del Cid, L., Chi, C.,
563         Escalona Segura, G., Gertsen, H., Salánki, T., van der Ploeg, M., Koelmans, A.A., Geissen, V.,
564         2017. Field evidence for transfer of plastic debris along a terrestrial food chain. Sci Rep 7,
565         14071. https://doi.org/10.1038/s41598-017-14588-2
566     Israelachvili, J.N., 2015. Intermolecular and surface forces.
567     Jambeck, J.R., Geyer, R., Wilcox, C., Siegler, T.R., Perryman, M., Andrady, A., Narayan, R., Law, K.L.,
568         2015. Plastic waste inputs from land into the ocean. Science 347, 768–771.
569         https://doi.org/10.1126/science.1260352
570     Jamieson, A.J., Malkocs, T., Piertney, S.B., Fujii, T., Zhang, Z., 2017. Bioaccumulation of persistent
571         organic pollutants in the deepest ocean fauna. Nat Ecol Evol 1, 51.
572         https://doi.org/10.1038/s41559-016-0051
573     Koelmans, A.A., 2019. Proxies for nanoplastic. Nature Nanotechnology 14, 307–308.
574         https://doi.org/10.1038/s41565-019-0416-z
575     Koelmans, Albert A., Besseling, E., Foekema, E., Kooi, M., Mintenig, S., Ossendorp, B.C., Redondo-
576         Hasselerharm, P.E., Verschoor, A., van Wezel, A.P., Scheffer, M., 2017. Risks of Plastic Debris:
577         Unravelling Fact, Opinion, Perception, and Belief. Environ. Sci. Technol. 51, 11513–11519.
578         https://doi.org/10.1021/acs.est.7b02219
579     Koelmans, Albert A, Kooi, M., Law, K.L., van Sebille, E., 2017. All is not lost: deriving a top-down mass
580         budget of plastic at sea. Environmental Research Letters 12, 114028.
581         https://doi.org/10.1088/1748-9326/aa9500
582     Lambert, S., Wagner, M., 2016. Characterisation of nanoplastics during the degradation of
583         polystyrene. Chemosphere 145, 265–268.
584         https://doi.org/10.1016/j.chemosphere.2015.11.078
585     Law, K.L., Moret-Ferguson, S., Maximenko, N.A., Proskurowski, G., Peacock, E.E., Hafner, J., Reddy,
586         C.M., 2010. Plastic Accumulation in the North Atlantic Subtropical Gyre. Science 329, 1185–
587         1188. https://doi.org/10.1126/science.1192321
588     Lecoanet, H.F., Bottero, J.-Y., Wiesner, M.R., 2004. Laboratory Assessment of the Mobility of
589         Nanomaterials in Porous Media. Environmental Science & Technology 38, 5164–5169.
590         https://doi.org/10.1021/es0352303
591     Lehner, R., Weder, C., Petri-Fink, A., Rothen-Rutishauser, B., 2019. Emergence of Nanoplastic in the
592         Environment and Possible Impact on Human Health. Environmental Science & Technology.
593         https://doi.org/10.1021/acs.est.8b05512
594     Liu, J., Zhang, T., Tian, L., Liu, X., Qi, Z., Ma, Y., Ji, R., Chen, W., 2019. Aging Significantly Affects
595         Mobility and Contaminant-mobilizing Ability of Nanoplastics in Saturated Loamy Sand.
596         Environ. Sci. Technol. acs.est.9b00787. https://doi.org/10.1021/acs.est.9b00787
597     McDowell-Boyer, L.M., Hunt, J.R., Sitar, N., 1986. Particle transport through porous media. Water
598         Resour. Res. 22, 1901–1921. https://doi.org/10.1029/WR022i013p01901
599     Ng, E.-L., Huerta Lwanga, E., Eldridge, S.M., Johnston, P., Hu, H.-W., Geissen, V., Chen, D., 2018. An
600         overview of microplastic and nanoplastic pollution in agroecosystems. Science of The Total
601         Environment 627, 1377–1388. https://doi.org/10.1016/j.scitotenv.2018.01.341
602     Obbard, R.W., Sadri, S., Wong, Y.Q., Khitun, A.A., Baker, I., Thompson, R.C., 2014. Global warming
603         releases microplastic legacy frozen in Arctic Sea ice. Earth's Future 2, 315–320.
604         https://doi.org/10.1002/2014EF000240
605     Pelley, A.J., Tufenkji, N., 2008. Effect of particle size and natural organic matter on the migration of
606         nano- and microscale latex particles in saturated porous media. Journal of Colloid and
607         Interface Science 321, 74–83. https://doi.org/10.1016/j.jcis.2008.01.046
608     Peng, G., Bellerby, R., Zhang, F., Sun, X., Li, D., 2020. The ocean's ultimate trashcan: Hadal trenches as
609         major depositories for plastic pollution. Water Research 168, 115121.
610         https://doi.org/10.1016/j.watres.2019.115121
611     Pessoni, L., Veclin, C., El Hadri, H., Cugnet, C., Davranche, M., Pierson-Wickmann, A.-C., Gigault, J.,
612         Grassl, B., Reynaud, S., 2019. Soap- and metal-free polystyrene latex particles as a
613         nanoplastic model. Environ. Sci.: Nano 6, 2253–2258. https://doi.org/10.1039/C9EN00384C

614 Petosa, A.R., Jaisi, D.P., Quevedo, I.R., Elimelech, M., Tufenkji, N., 2010. Aggregation and Deposition
615　　　of Engineered Nanomaterials in Aquatic Environments: Role of Physicochemical Interactions.
616　　　Environmental Science & Technology 44, 6532–6549. https://doi.org/10.1021/es100598h

617 Quevedo, I.R., Tufenkji, N., 2012. Mobility of Functionalized Quantum Dots and a Model Polystyrene
618　　　Nanoparticle in Saturated Quartz Sand and Loamy Sand. Environmental Science &
619　　　Technology 46, 4449–4457. https://doi.org/10.1021/es2045458

620 Redman, J.A., Walker, S.L., Elimelech, M., 2004. Bacterial Adhesion and Transport in Porous Media:
621　　　Role of the Secondary Energy Minimum. Environ. Sci. Technol. 38, 1777–1785.
622　　　https://doi.org/10.1021/es034887l

623 Rillig, M.C., 2012. Microplastic in Terrestrial Ecosystems and the Soil? Environmental Science &
624　　　Technology 46, 6453–6454. https://doi.org/10.1021/es302011r

625 Salerno, M.B., Flamm, M., Logan, B.E., Velegol, D., 2006. Transport of Rodlike Colloids through
626　　　Packed Beds. Environ. Sci. Technol. 40, 6336–6340. https://doi.org/10.1021/es0614565

627 Scheurer, M., Bigalke, M., 2018. Microplastics in Swiss Floodplain Soils. Environ. Sci. Technol. 52,
628　　　3591–3598. https://doi.org/10.1021/acs.est.7b06003

629 Schwarz, A.E., Ligthart, T.N., Boukris, E., van Harmelen, T., 2019. Sources, transport, and
630　　　accumulation of different types of plastic litter in aquatic environments: A review study.
631　　　Marine Pollution Bulletin 143, 92–100. https://doi.org/10.1016/j.marpolbul.2019.04.029

632 Seymour, M.B., Chen, G., Su, C., Li, Y., 2013. Transport and Retention of Colloids in Porous Media:
633　　　Does Shape Really Matter? Environ. Sci. Technol. 130722083052008.
634　　　https://doi.org/10.1021/es4016124

635 Syngouna, V.I., Chrysikopoulos, C.V., 2013. Cotransport of clay colloids and viruses in water saturated
636　　　porous media. Colloids and Surfaces A: Physicochemical and Engineering Aspects 416, 56–65.
637　　　https://doi.org/10.1016/j.colsurfa.2012.10.018

638 Ter Halle, A., Jeanneau, L., Martignac, M., Jardé, E., Pedrono, B., Brach, L., Gigault, J., 2017.
639　　　Nanoplastic in the North Atlantic Subtropical Gyre. Environmental Science & Technology 51,
640　　　13689–13697. https://doi.org/10.1021/acs.est.7b03667

641 Tong, M., Johnson, W.P., 2006. Excess Colloid Retention in Porous Media as a Function of Colloid
642　　　Size, Fluid Velocity, and Grain Angularity. Environ. Sci. Technol. 40, 7725–7731.
643　　　https://doi.org/10.1021/es061201r

644 Treumann, S., Torkzaban, S., Bradford, S.A., Visalakshan, R.M., Page, D., 2014. An explanation for
645　　　differences in the process of colloid adsorption in batch and column studies. Journal of
646　　　Contaminant Hydrology 164, 219–229. https://doi.org/10.1016/j.jconhyd.2014.06.007

647 Tufenkji, N., Elimelech, M., 2005. Breakdown of Colloid Filtration Theory: Role of the Secondary
648　　　Energy Minimum and Surface Charge Heterogeneities. Langmuir 21, 841–852.
649　　　https://doi.org/10.1021/la048102g

650 Tufenkji, N., Elimelech, M., 2004. Correlation Equation for Predicting Single-Collector Efficiency in
651　　　Physicochemical Filtration in Saturated Porous Media. Environmental Science & Technology
652　　　38, 529–536. https://doi.org/10.1021/es034049r

653 Valsesia, A., Desmet, C., Ojea-Jiménez, I., Oddo, A., Capomaccio, R., Rossi, F., Colpo, P., 2018. Direct
654　　　quantification of nanoparticle surface hydrophobicity. Commun Chem 1, 53.
655　　　https://doi.org/10.1038/s42004-018-0054-7

656 van Sebille, E., Wilcox, C., Lebreton, L., Maximenko, N., Hardesty, B.D., van Franeker, J.A., Eriksen, M.,
657　　　Siegel, D., Galgani, F., Law, K.L., 2015. A global inventory of small floating plastic debris.
658　　　Environmental Research Letters 10, 124006. https://doi.org/10.1088/1748-
659　　　9326/10/12/124006

660 Verleysen, E., Wagner, T., Lipinski, H.-G., Kägi, R., Koeber, R., Boix-Sanfeliu, A., De Temmerman, P.-J.,
661　　　Mast, J., 2019. Evaluation of a TEM based Approach for Size Measurement of Particulate
662　　　(Nano)materials. Materials 12, 2274. https://doi.org/10.3390/ma12142274

663 Vinogradov, J., Jaafar, M.Z., Jackson, M.D., 2010. Measurement of streaming potential coupling
664　　　coefficient in sandstones saturated with natural and artificial brines at high salinity. J.
665　　　Geophys. Res. 115, B12204. https://doi.org/10.1029/2010JB007593

666    Wagner, M., Scherer, C., Alvarez-Muñoz, D., Brennholt, N., Bourrain, X., Buchinger, S., Fries, E.,
667            Grosbois, C., Klasmeier, J., Marti, T., Rodriguez-Mozaz, S., Urbatzka, R., Vethaak, A.D.,
668            Winther-Nielsen, M., Reifferscheid, G., 2014. Microplastics in freshwater ecosystems: what
669            we know and what we need to know. Environmental Sciences Europe 26.
670            https://doi.org/10.1186/s12302-014-0012-7
671    Wagner, S., Reemtsma, T., 2019. Things we know and don't know about nanoplastic in the
672            environment. Nature Nanotechnology 14, 300–301. https://doi.org/10.1038/s41565-019-
673            0424-z
674    Weiss, T.H., Mills, A.L., Hornberger, G.M., Herman, J.S., 1995. Effect of Bacterial Cell Shape on
675            Transport of Bacteria in Porous Media. Environ. Sci. Technol. 29, 1737–1740.
676            https://doi.org/10.1021/es00007a007
677    Wu, J., Jiang, R., Lin, W., Ouyang, G., 2019. Effect of salinity and humic acid on the aggregation and
678            toxicity of polystyrene nanoplastics with different functional groups and charges.
679            Environmental Pollution 245, 836–843. https://doi.org/10.1016/j.envpol.2018.11.055
680    Wu, L., Gao, B., Tian, Y., Muñoz-Carpena, R., Zigler, K.J., 2013. DLVO Interactions of Carbon
681            Nanotubes with Isotropic Planar Surfaces. Langmuir 29, 3976–3988.
682            https://doi.org/10.1021/la3048328
683    Xu, S., Liao, Q., Saiers, J.E., 2008. Straining of nonspherical colloids in saturated porous media.
684            Environ. Sci. Technol. 42, 771–778. https://doi.org/10.1021/es071328w
685

**Deposition of Environmentally Relevant Nanoplastic Models in Sand during Transport**

**Experiments**

Alice Pradel [a*], Hind el Hadri [b], Cloé Desmet[c], Jessica Ponti[c], Stéphanie Reynaud [b], Bruno Grassl [b], Julien Gigault [a*]

[a] *Univ Rennes, CNRS, Géosciences Rennes - UMR 6118, 35000 Rennes, France*
[b] *IPREM, UMR 5254, CNRS-Université de Pau et des Pays de L'Adour, 64000 Pau, France*
[c] *European Commission, Joint Research Centre (JRC), Directorate F - Health, Consumers and Reference Materials, Via E. Fermi 2749, 21027 Ispra, VA, Italy*
*julien.gigault@univ-rennes1.fr*

**Highlights**

- In order to determine the environmental fate of nanoplastics, models of nanoplastics with environmentally relevant physicochemical properties must be used.
- Nanoplastic models with polymorphic (irregular and asymmetrical) shapes are more likely to be trapped in porous media, than spherical models.
- Shape has a greater impact on the deposition rate than particle size or particle concentration.

**Deposition of Environmentally Relevant Nanoplastic Models in Sand during Transport**

**Experiments**

Alice Pradel [a*], Hind el Hadri [b], Cloé Desmet[c], Jessica Ponti[c], Stéphanie Reynaud [b], Bruno Grassl [b], Julien Gigault [a*]

[a] *Univ Rennes, CNRS, Géosciences Rennes - UMR 6118, 35000 Rennes, France*

[b] *IPREM, UMR 5254, CNRS-Université de Pau et des Pays de L'Adour, 64000 Pau, France*

[c] *European Commission, Joint Research Centre (JRC), Directorate F - Health, Consumers and Reference Materials, Via E. Fermi 2749, 21027 Ispra, VA, Italy*

*\*julien.gigault@univ-rennes1.fr*

**Declaration of interests**

☒ The authors declare that they have no known competing financial interests or personal relationships that could have appeared to influence the work reported in this paper.

☐The authors declare the following financial interests/personal relationships which may be considered as potential competing interests: